Icarus 209 (2010) 239–246

Contents lists available at ScienceDirect

Icarus

journal homepage: www.elsevier.com/locate/icarus

# The apparent lack of lunar-like swirls on Mercury: Implications for the formation of lunar swirls and for the agent of space weathering

David T. Blewett [a,*], Brett W. Denevi [b], Mark S. Robinson [b], Carolyn M. Ernst [a], Michael E. Purucker [c], Sean C. Solomon [d]

[a] Johns Hopkins University, Applied Physics Laboratory, 11100 Johns Hopkins Road, Laurel, MD 20723, USA
[b] School of Earth and Space Exploration, Arizona State University, Tempe, AZ 85287, USA
[c] Raytheon/NASA Goddard Space Flight Center, Greenbelt, MD 20771, USA
[d] Department of Terrestrial Magnetism, Carnegie Institution of Washington, Washington, DC 20015, USA

ARTICLE INFO

*Article history:*
Received 23 July 2009
Revised 10 March 2010
Accepted 11 March 2010
Available online 15 March 2010

*Keywords:*
Mercury, Surface
Moon, Surface
Solar wind
Magnetic fields

ABSTRACT

Images returned by the MESSENGER spacecraft from the Mercury flybys have been examined to search for anomalous high-albedo markings similar to lunar swirls. Several features suggested to be swirls on the basis of Mariner 10 imaging (in the craters Handel and Lermontov) are seen in higher-resolution MESSENGER images to lack the characteristic morphology of lunar swirls. Although antipodes of large impact basins on the Moon are correlated with swirls, the antipodes of the large impact basins on Mercury appear to lack unusual albedo markings. The antipodes of Mercury's Rembrandt, Beethoven, and Tolstoj basins do not have surface textures similar to the "hilly and lineated" terrain found at the Caloris antipode, possibly because these three impacts were too small to produce obvious surface disturbances at their antipodes. Mercury does have a class of unusual high-reflectance features, the bright crater-floor deposits (BCFDs). However, the BCFDs are spectral outliers, not simply optically immature material, which implies the presence of material with an unusual composition or physical state. The BCFDs are thus not analogs to the lunar swirls. We suggest that the lack of lunar-type swirls on Mercury supports models for the formation of lunar swirls that invoke interaction between the solar wind and crustal magnetic anomalies (i.e., the solar-wind standoff model and the electrostatic dust-transport model) rather than those models of swirl formation that relate to cometary impact phenomena. If the solar-wind standoff hypothesis for lunar swirls is correct, it implies that the primary agent responsible for the optical effects of space weathering on the Moon is solar-wind ion bombardment rather than micrometeoroid impact.


## 1. Introduction

Lunar swirls are sinuous, high-albedo markings that have no apparent topographic expression, are not topographically controlled, and appear to overprint the surfaces on which they lie (El-Baz, 1972; Schultz and Srnka, 1980). The most famous example is the Reiner Gamma formation in western Oceanus Procellarum. As illustrated by the Mare Ingenii swirls (Fig. 1), the unusual patterns are prominent against the dark mare basalt background. Swirls are also found on the lunar highlands (e.g., El-Baz, 1972; Hood and Williams, 1989; Richmond et al., 2003; Blewett et al., 2007). Some swirls have been identified as having anomalous photometric properties (e.g., Kreslavsky and Shkuratov, 2003; Kaydash et al., 2009; Shkuratov et al., 2010).

Several hypotheses for the origin of lunar swirls have been proposed. Early conjectures attributed the high-albedo markings to nuée ardente deposits (McCauley, 1967), or to material derived from sublimation of volatiles from the lunar interior (e.g., Whitaker, 1969; El-Baz, 1972; Schultz, 1976). Later ideas incorporated the association between swirls and crustal magnetic anomalies, which were discovered from Apollo subsatellite data (e.g., Coleman et al., 1972; Russell et al., 1975; Hood et al., 1981). A leading hypothesis is that the magnetic anomaly protects the surface from solar-wind ion bombardment. According to this hypothesis (Hood and Schubert, 1980; Hood and Williams, 1989; Hood et al., 2001), a protected area experiences substantially reduced solar-wind sputtering and implantation and thus does not undergo the normal space-weathering process to which unshielded areas are subjected. Thus it may be that the presence of a magnetic anomaly maintains the high albedo of unweathered material exposed by impacts. In addition, immature ray material originating at distant impacts that is deposited within the magnetically shielded area could contribute to the high-reflectance of the swirl (e.g., Hood

* Corresponding author. Fax: +1 443 778 8939.
*E-mail addresses:* david.blewett@jhuapl.edu (D.T. Blewett), bdenevi@ser.asu.edu (B.W. Denevi), robinson@ser.asu.edu (M.S. Robinson), carolyn.ernst@jhuapl.edu (C.M. Ernst), Michael.E.Purucker@nasa.gov (M.E. Purucker), scs@dtm.ciw.edu (S.C. Solomon).

0019-1035/$ - see front matter © 2010 Elsevier Inc. All rights reserved.
doi:10.1016/j.icarus.2010.03.008

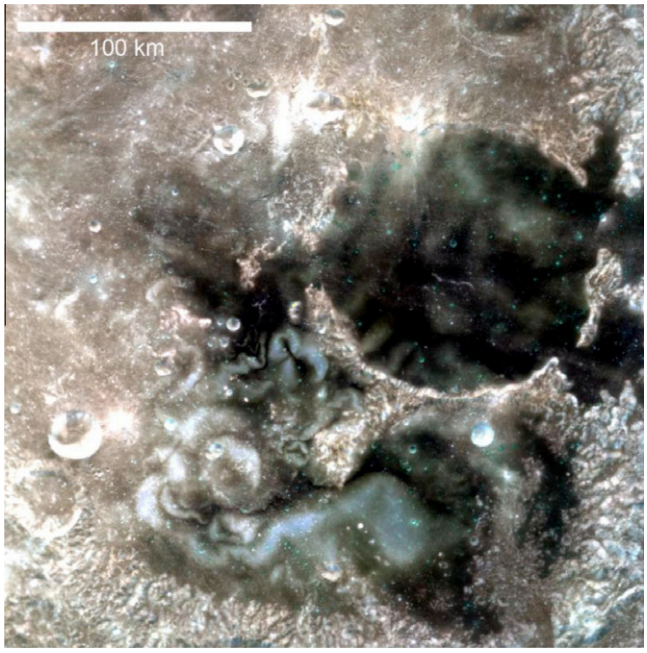


**Fig. 1.** Lunar swirls on the lunar farside near the antipode to the Imbrium basin. Clementine color composite of images taken through 950-, 750-, 415-nm filters in the red, green, and blue image planes, respectively. The image has north toward the top and is centered at ~33°S, 164°E. Sinuous, high-reflectance swirl markings are most prominent on the low-reflectance areas of Mare Ingenii and may cross adjacent highland terrain. A strong crustal magnetic anomaly is found in this region (e.g., Lin et al., 1988; Hood et al., 2001; Richmond et al., 2005).

et al., 1979; Hood and Williams, 1989). Micrometeoroid bombardment is also considered to be an agent of space weathering (e.g., Hapke, 2001). However, micrometeoroids would not be affected by the presence of a crustal magnetic field (Richmond et al., 2003).

A second hypothesis for the origin of lunar swirls that requires the interaction of the solar wind with a crustal magnetic anomaly has recently been proposed (Garrick-Bethell et al., 2009, 2010). According to this mechanism, the magnetic anomalies give rise to weak electric fields when solar wind protons and electrons penetrate to different depths in the magnetic field. At the surface, the electric fields could cause selective attraction and repulsion of fine, electrostatically levitated dust grains, resulting in concentrations of fine, high-albedo, feldspar-rich dust that form the bright portions of the swirls.

Many, though not all, lunar crustal magnetic anomalies are correlated with terranes antipodal to a major impact basin (e.g., Lin et al., 1988; Halekas et al., 2001; Richmond et al., 2005). The creation of a crustal magnetic anomaly may involve the amplification of existing magnetic fields by the expanding vapor-melt cloud produced in a lunar basin-forming impact (Hood and Artemieva, 2008).

The other major concept for the formation of swirls invokes surface effects produced during the relatively recent (<1 Ma) impact of a comet coma and nucleus (Schultz and Srnka, 1980), disrupted comet fragments (Pinet et al., 2000), or a cometary meteor swarm (Starukhina and Shkuratov, 2004). Under this scenario, the surface magnetization results from alteration of the regolith and thermal and/or shock remanence in the presence of the cometary field (Gold and Soter, 1976; Schultz and Srnka, 1980).

In their discussion of the comet-impact hypothesis for lunar swirls, Schultz and Srnka (1980) suggested that swirl-like markings exist on Mercury. The availability of higher-resolution, higher-quality images from the flybys of Mercury by the MErcury Surface, Space ENvironment, GEochemistry, and Ranging (MESSENGER) spacecraft (Solomon et al., 2008; Robinson et al., 2008; Chabot et al., 2008; Becker et al., 2009) now allow us to re-examine the suggested swirl features on Mercury, as well as to search for additional swirl candidates. Analysis of these observations of Mercury thus permits an assessment of the proposed hypotheses for the origin of swirls on the Moon. Comet impacts should occur on Mercury (e.g., Gold and Soter, 1976), so if the comet-impact model for lunar swirl formation is correct, Mercury should also exhibit swirls. Starukhina and Shkuratov (2004), for instance, predicted that swirls (produced in shallow "plowing" impacts by cometary meteor swarms) are more common on Mercury than on the Moon,

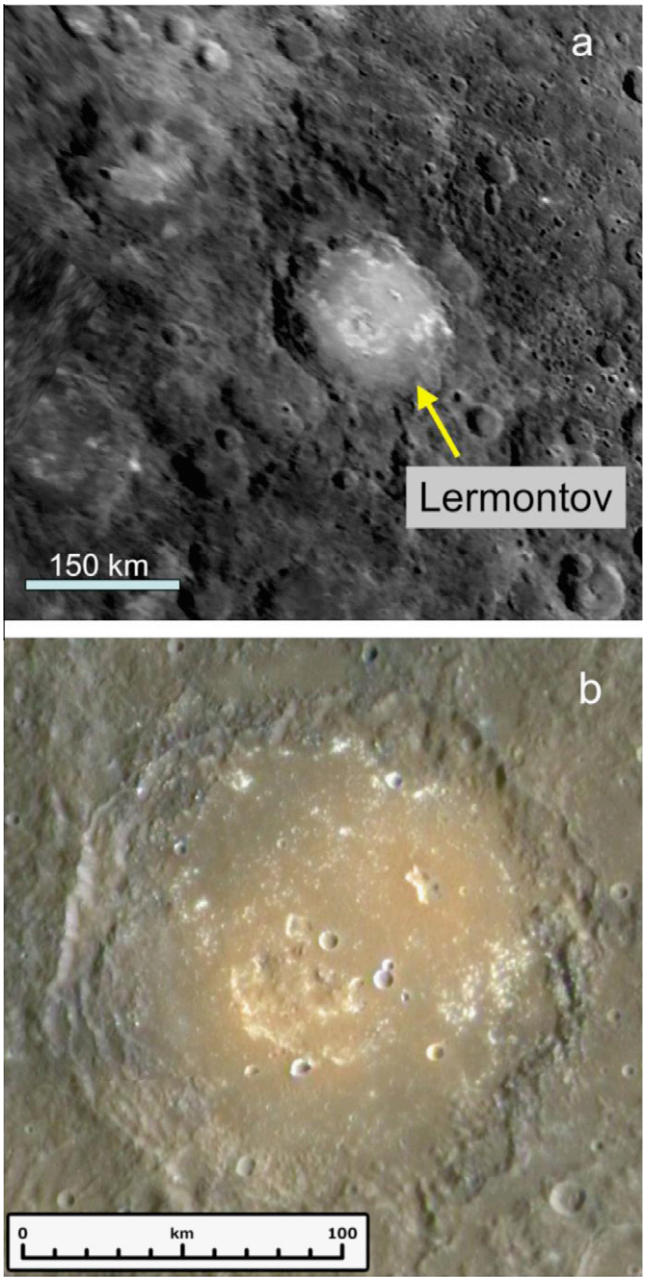


**Fig. 2.** Lermontov crater, Mercury (152 km in diameter, crater centered at 15°N, 311°E). (a) Mariner 10 clear-filter image, resolution 1 km/pixel (Denevi and Robinson, 2008). (b) MESSENGER NAC image (~250 m/pixel, from second Mercury encounter "departure mosaic 2") enhanced with WAC color (R = 1020 nm, G = 700 nm, B = 430 nm). The "swirl-like" markings in the lower-resolution Mariner 10 image are seen from the NAC image to have been produced by Sun-facing walls of irregular depressions and numerous small bright spots and impact craters. North is toward the top in both images.

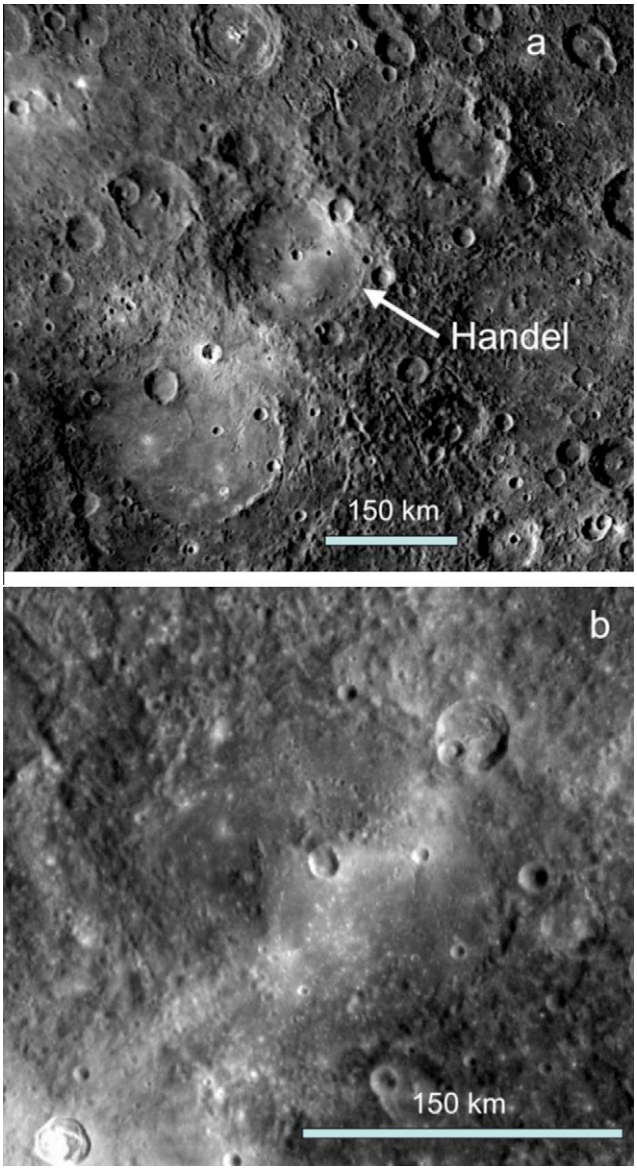


**Fig. 3.** Handel crater, Mercury (166 km in diameter, crater centered at 4°N, 325°E). (a) Mariner 10 clear-filter image, resolution 1 km/pixel (Denevi and Robinson, 2008). (b) MESSENGER NAC image (~250 m/pixel, from second Mercury encounter "departure mosaic 2"). The diffuse band crossing Handel's floor is seen in the NAC image to be caused by ray segments from Dominici crater to the southwest and a smaller impact on the Handel floor. North is toward the top in both images.

because of more frequent swarm encounters and the presence of denser clouds of cometary debris closer to the Sun (see also Gold and Soter, 1976). Therefore, a failure to identify swirls on Mercury would be evidence against the comet-impact hypothesis for lunar swirl formation.

## 2. Candidate swirls on Mercury

The "bright loops and swirls" reported by Schultz and Srnka (1980) are in or near the craters Lermontov and Handel. Lermontov has a relatively high-albedo floor that contains bright streaks in Mariner 10 images (Fig. 2a). The floor of Handel as seen by Mariner 10 (Fig. 3a) is crossed by a curving, diffuse, bright band.

Images obtained by MESSENGER during its flybys of Mercury were acquired with the Mercury Dual Imaging System (MDIS) (Hawkins et al., 2007). MDIS consists of a narrow-angle camera (NAC) that provides monochrome imaging (through a broadband filter centered at ~750 nm wavelength), and a wide-angle camera (WAC) that collects multispectral images through 11 narrow-band filters with wavelength centers between ~430 and 1020 nm.

MESSENGER NAC images reveal the markings on Lermontov's floor noted by Schultz and Srnka (1980) to be irregular depressions and small unresolved bright spots (Fig. 2b). The floor displays a spectral reflectance that increases strongly with wavelength relative to the global average, i.e., an anomalous red color (Dzurisin, 1977; Schultz, 1977; Rava and Hapke, 1987; Robinson and Lucey, 1997; Blewett et al., 2007, 2008). Elsewhere on Mercury, similar relatively high-reflectance, red material associated with irregular depressions has been interpreted to be of pyroclastic origin (Robinson et al., 2008; Head et al., 2008, 2009; Murchie et al., 2008; Kerber et al., 2009). The high-resolution MESSENGER data show that no features resembling lunar swirls are present on the floor of Lermontov, although the area is a candidate for past explosive volcanism.

The MESSENGER NAC image of Handel (Fig. 3b) shows that the marking noted by Schultz and Srnka (1980) is likely a result of ordinary ray segments from a nearby crater (Dominici) and from a small impact crater on the floor. No loops or sinuous bright or dark bands are seen in the higher-resolution data. Hence, the improved imaging reveals that the Handel location does not possess the characteristics of a lunar swirl.

## 3. Basin antipodes on Mercury

Inasmuch as a correlation between albedo anomalies and basin antipodes is found on the Moon (Lin et al., 1988; Richmond et al., 2005), an interesting question is whether such an association occurs on Mercury. The Caloris basin (~1550 km diameter,

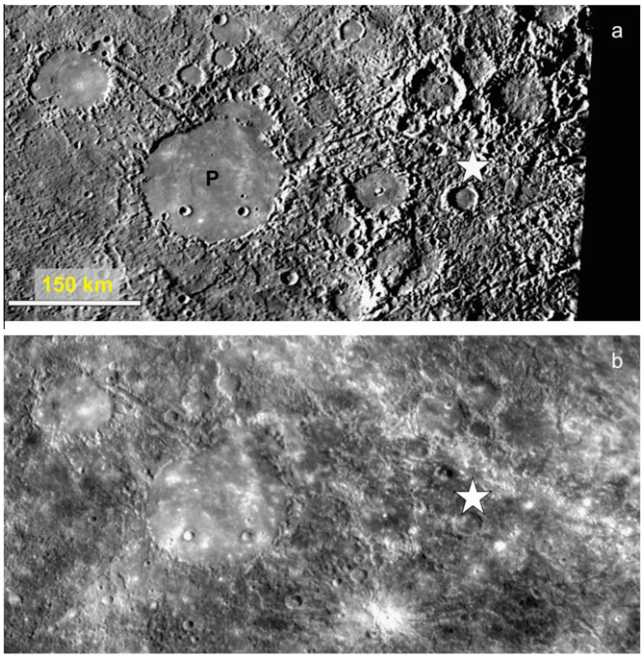


**Fig. 4.** The area of the Caloris basin antipode, Mercury. Both images cover ~25–35°S, 327–347°E and have north toward the top. The geometrical location of the antipode is marked by the star (~30°S, 341.5°E). "P" is the crater Petrarch. (a) Mariner 10 clear-filter view (Denevi and Robinson, 2008); low-Sun illumination emphasizes topography. The surface in the "hilly and lineated" terrain (Murray et al., 1974) has been broken up into hills 5–10 km wide and 0.1–1.8 km high. (b) MESSENGER NAC image (from second Mercury encounter "departure mosaic 3"); high-Sun illumination emphasizes albedo differences. High-reflectance patterns are attributable to large and small crater rays and topography, with no definitive examples of the morphology characteristic of lunar swirls.

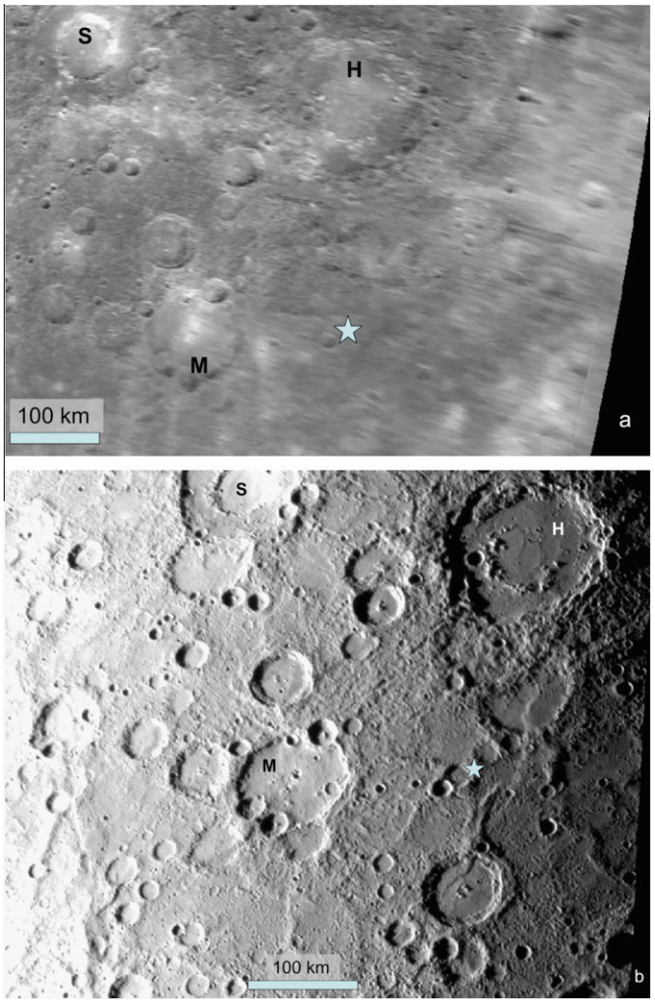


**Fig. 5.** The area antipodal to the Rembrandt basin, Mercury. The star is at the basin's geometrical antipode (~33°N, 268°E). (a) Mariner 10 clear-filter mosaic (Denevi and Robinson, 2008) in sinusoidal projection with north toward the top, covering ~30–42°N, ~256–277°E. (b) MESSENGER first flyby NAC approach image in orthographic projection with north toward the top, covering ~27–41°N, 254–273°E. The following craters are labeled: "S" = Scarlatti, "M" = Mussorgskij, "H" = al-Hamadhani.

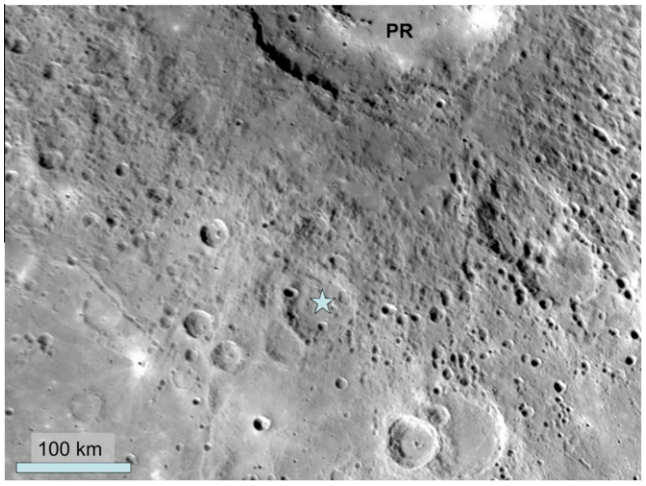


**Fig. 6.** The area antipodal to the Beethoven basin, Mercury. The star is at the Beethoven basin's geometrical antipode (~20°N, 56°E). MESSENGER third flyby NAC approach image in sinusoidal projection with north toward the top, covering 16.3–26.3°N, 49–63°E. The formation of the peak-ring Rachmaninoff basin ("PR") and plains volcanism have strongly affected the area of Beethoven's antipode.

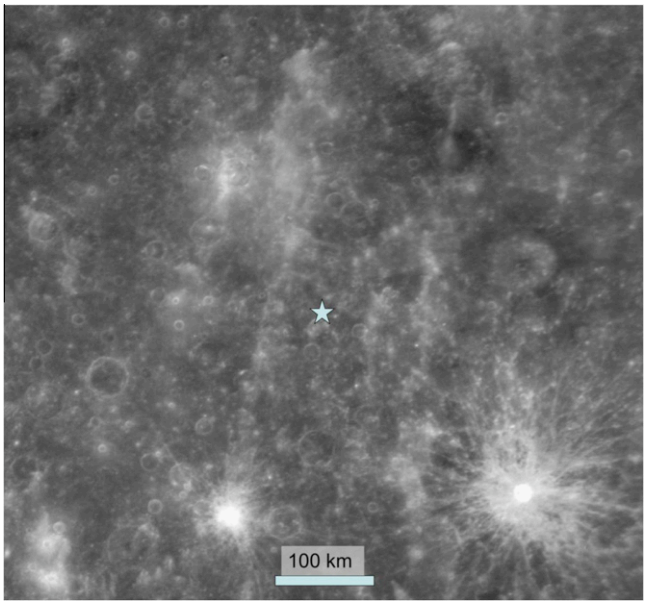


**Fig. 7.** The area antipodal to the Tolstoj basin, Mercury. MESSENGER NAC image (from second Mercury encounter "departure mosaic 3") in simple cylindrical projection with north toward the top, covering ~9–24°N, 8–24°E. The star is at the basin's geometrical antipode (~16°N, 16°E). No obvious albedo anomalies are present. The texture characteristic of the Caloris antipode's "hilly and lineated" terrain (cf. Fig. 4b) is not apparent.

Murchie et al., 2008) is the youngest large basin on Mercury. "Hilly and lineated" terrain (Murray et al., 1974) located at the Caloris antipode (~30°S, 341.5°E, Fig. 4) may have been formed by converging seismic waves (Schultz and Gault, 1975; Hughes et al., 1977) or ejecta (Moore et al., 1974) from the Caloris impact. An ejecta-deposition origin for the antipodal terrain was favored by Wieczorek and Zuber (2001). Similar grooved and broken-up terrain is found at the antipode of the lunar Imbrium basin (Fig. 1; Moore et al., 1974; Schultz and Gault, 1975; Stuart-Alexander, 1978), suggesting that similar processes accompanied the formation of these two basins.

The area of the Caloris antipode has been imaged at both high- and low-Sun illumination (Fig. 4). Several high-reflectance crater rays cross the area of the Caloris antipode (Fig. 4b), which together with the unusual texture of the terrain potentially makes recognition of anomalous albedo patterns difficult. However, no markings with the complex geometry of the lunar Reiner Gamma or Mare Ingenii swirls are apparent.

Other large, relatively young basins on Mercury include Rembrandt (715-km diameter, Calorian age, Watters et al., 2009), Tolstoj (510-km diameter, Tolstojan age, Spudis and Guest, 1988), and Beethoven (625-km diameter, Tolstojan age, intermediate between Caloris and Tolstoj, Spudis and Guest, 1988). The Rembrandt antipode (~33°N, 268°E) is currently covered by only poor-resolution Mariner 10 images (Fig. 5a) and data near the terminator obtained during the first MESSENGER flyby approach sequence (Fig. 5b). For the Beethoven antipode (~20°N, 56°E), the best views are from MESSENGER's third flyby approach (Fig. 6). Tolstoj's antipodal region (~16°N, 16°E) was visible in MESSENGER second flyby departure images at high-Sun illumination (Fig. 7). The area of the Beethoven antipode has been heavily modified by the formation of a nearby peak-ring basin (Rachmaninoff, Prockter et al., 2010); smooth plains emplacement predating the peak-ring basin and the deposition of its ejecta could have obscured any characteristic antipodal morphology that may have been produced by

**Table 1**
Selected large impact basins on Mercury and the Moon.

| Basin name | Basin diameter, km[a] | Basin diameter/target diameter[b] |
|---|---|---|
| Caloris | 1550 | 0.32 |
| Rembrandt | 715 | 0.15 |
| Beethoven | 625 | 0.13 |
| Tolstoj | 510 | 0.10 |
| Imbrium | 1160 | 0.33 |
| Orientale | 930 | 0.27 |
| Serenitatis | 920 | 0.26 |
| Crisium | 740 | 0.21 |

[a] For Mercury basin diameter references, see text. Lunar basin diameters from Table 2.1 of Spudis (1993).
[b] Target body diameters: Mercury, 4880 km; Moon, 3476 km.

Beethoven. No albedo markings reminiscent of lunar swirls are found at the Beethoven antipode. The Rembrandt and Tolstoj antipodal regions appear to lack both swirl-like albedo anomalies and "hilly and lineated"-type terrain.

The available imaging for the antipodes of Rembrandt, Beethoven, and Tolstoj basins is less than complete. Regardless, these basins may be too small to produce major effects on the antipodal geology. Unusual antipodal terrain morphology has been described for the lunar basins Imbrium, Orientale, Serenitatis, and Crisium (e.g., Wilhelms, 1987). Table 1 lists the diameters of the main rims of these four basins and comparable basins on Mercury, along with the ratio of the basin diameter to the diameter of the target object. The table shows that Rembrandt, Beethoven, and Tolstoj are smaller relative to the size of the target body than are the four lunar basins for which characteristic antipodal terrain has been documented. The greater volume and surface gravity, and the different interior structure of Mercury compared with the Moon, could be other factors that inhibit generation of antipodal effects by these smaller basins. The antipodes of all listed basins on Mercury can be imaged with differing viewing geometries and higher spatial resolution during the orbital phase of the MESSENGER mission to test the preliminary assessment given here.

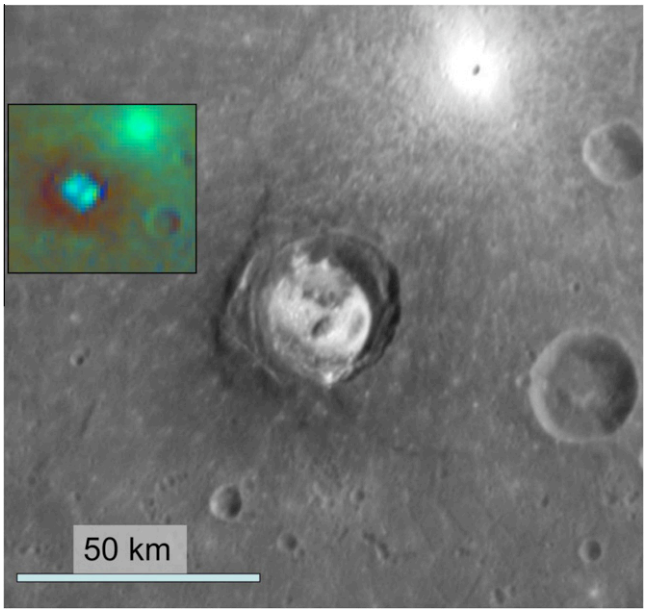


**Fig. 8.** Kertész crater, Mercury (33 km in diameter, centered at 27.4°N, 146.0°E). MESSENGER first flyby NAC departure image in orthographic projection with north toward the top. Inset: MESSENGER first flyby WAC color-composite image with the following color assignments: red image plane = 630-nm/430-nm ratio, green plane = 560-nm reflectance, blue plane = 430-nm/630-nm ratio. Red-to-blue pixel variations relate to the spectral slope (redder = steeper, bluer = shallower). The floor of Kertész contains bright crater-floor deposits (BCFDs). The BCFD material is noticeably bluer than the ejecta of the small fresh crater at the upper right.

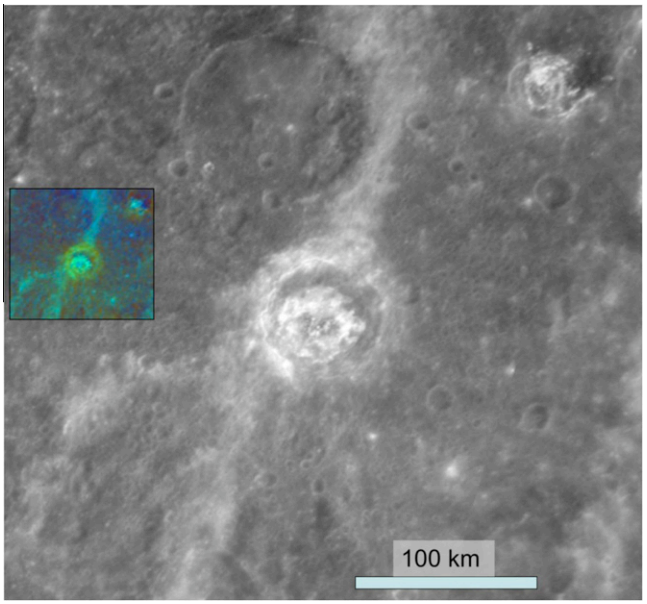


**Fig. 9.** The crater de Graft, Mercury (65 km in diameter, centered at 22.1°N, 2.0°E), containing BCFD material. MESSENGER second flyby departure NAC image from "departure mosaic 3" with north toward the top; inset shows WAC color-composite image with the following color assignments: red image plane = 630-nm/430-nm ratio, green plane = 560-nm reflectance, blue plane = 430-nm/630-nm ratio. Red-to-blue pixel variations relate to the spectral slope (redder = steeper, bluer = shallower). The floor of the crater is occupied by bright crater-floor deposits (BCFDs). Similar material is found in the smaller crater at the upper right. Two nearly parallel rays from a large crater to the northeast cross the image at center and lower right.

## 4. Bright crater-floor deposits on Mercury

Although we have not found counterparts to lunar swirls on Mercury, there does exist a class of enigmatic high-albedo markings. The "bright crater-floor deposits" (BCFDs) (Robinson et al., 2008; Blewett et al., 2009) are characterized by high-reflectance and a spectral slope in the visible to near-infrared that is very shallow ("blue") compared with the global average. Examples of these deposits were imaged during MESSENGER's first and second Mercury flybys and are found on the floors of craters such as Kertész and de Graft (Figs. 8 and 9) and associated with the peak-ring mountains of Eminescu and Raditladi. Crater floor materials with similar albedo and color properties were also identified in Mariner 10 color images (Dzurisin, 1977; Schultz, 1977; Rava and Hapke, 1987). Examples include the craters Balzac, Tyagaraja, and Zeami (Fig. 10). These three craters were not illuminated during the MESSENGER flybys. The BCFDs do not have the wispy, diffuse appearance of lunar swirls. Rather, the BCFDs are more characteristic of exposures or deposits of a coherent material, in some cases with flow-like boundaries.

The association with crater interiors and the flow-like boundaries of some BCFDs (Figs. 8 and 9) could indicate that the deposits are related to impact melts. Meteoroid impact speeds at Mercury are thought to be considerably higher than at the Moon. Le Feuvre and Wieczorek (2008) report the average speed to be 42 km/s for Mercury, versus 19 km/s for the Moon. Marchi et al. (2005) give an average impact speed of 30 km/s for Mercury, with the range spanning 15–80 km/s. High-velocity impacts should produce higher proportions of melting (e.g., Cintala, 1992). Craters formed in especially energetic events could have thick deposits of impact-generated magma on their floors.

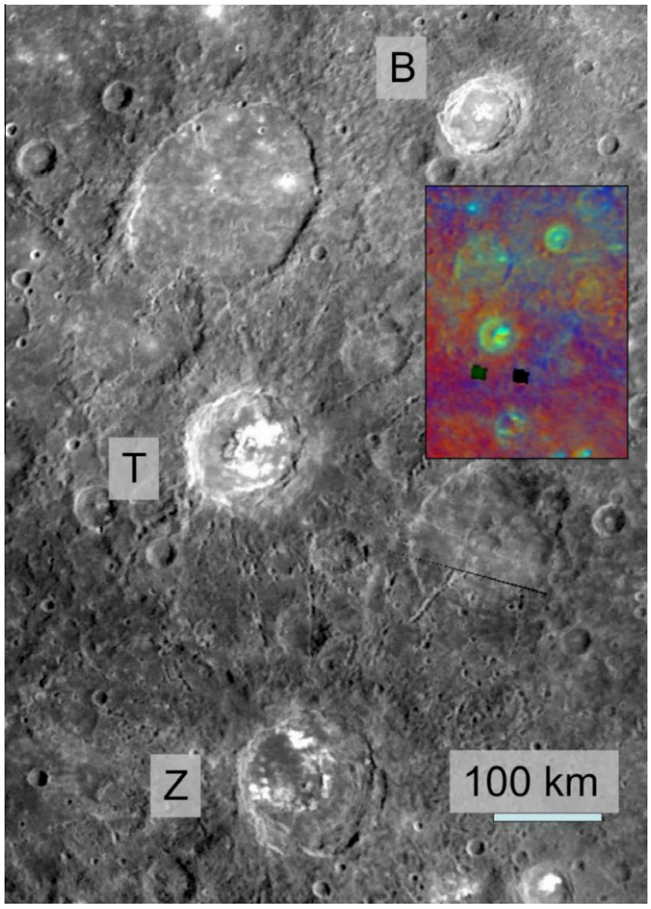


**Fig. 10.** Mariner 10 clear-filter mosaic (Denevi and Robinson, 2008) of the area of craters Balzac (B), Tyagaraja (T), and Zeami (Z) in sinusoidal projection covering ~5.4° S–13°N, 207–219°E. The inset is a Mariner 10 color-composite image covering the same area, with the following color assignments: red image plane = 575-nm/355-nm ratio, green plane = 575-nm reflectance, blue plane = 355-nm/575-nm ratio. Red-to-blue pixel variations relate to the spectral slope (redder = steeper, bluer = shallower). These three craters have high-reflectance, relatively blue BCFD material on their floors and central peaks.

On the other hand, the occurrence of BCFD material on some central peak mountains implies that at least some such material originally resided at depth and was uplifted during the rebound phase of crater formation (e.g., Cintala and Grieve, 1998; Melosh, 1989). Previous speculations on the origin of bright crater material on Mercury include that of Schultz (1977), who mentioned the possibility that intensely shock-altered material in the crater floors could be responsible for the albedo and color properties. Dzurisin (1977) suggested that fumarolic activity along impact-generated fractures might have produced physical or chemical alteration leading to the characteristic color and albedo.

On spectral grounds, it is likely that BCFD material and lunar swirl material have distinct origins. The high-reflectance portions of lunar swirls have spectral characteristics consistent with those of typical immature regolith. For example, at Reiner Gamma, the bright swirl patterns are dominated by optically immature mare material (Bell and Hawke, 1981, 1987; Pinet et al., 2000). Similarly, Blewett et al. (2005) found that optical maturity differences account for an albedo anomaly in the Descartes highlands that is co-located with a crustal magnetic anomaly (see also Richmond et al., 2003). This characteristic contrasts with Mercury's BCFDs. The BCFDs are global spectral outliers that do not fall along the maturation trends of the major crustal color units on Mercury (Blewett et al., 2009), strongly suggesting a compositional difference from the great majority of the planet's surface. It is unlikely that the BCFDs owe their spectral characteristics solely to the presence of immature material, especially since many BCFDs are found in older, large craters. Furthermore, lunar swirls are not confined to crater interiors, as appears to be the case with BCFDs. Accordingly, the BCFDs are not analogs on Mercury to swirls on the Moon. No lunar analog to the BCFDs is known, perhaps because of differences in target composition and impact velocity. Future data collected during MESSENGER orbital operations around Mercury, including MDIS stereo imaging and spectra obtained by the Mercury Atmospheric and Surface Composition Spectrometer (MASCS, McClintock and Lankton, 2007) may provide additional insight into the nature of the unusual BCFD material.

## 5. Discussion

Combined Mariner 10 and MESSENGER imaging now covers more than 97% of the surface of Mercury (Becker et al., 2009; see description of the global mosaic at http://astrogeology.usgs.gov/Projects/Messenger/). A survey of MESSENGER NAC images from the flybys has not revealed any features with the classic lunar swirl morphology. We therefore conclude, pending additional future observations, that swirls of the lunar type do not occur on Mercury.

As mentioned above, because comets strike Mercury, perhaps with greater frequency than they do the Moon (e.g., Gold and Soter, 1976; Starukhina and Shkuratov, 2004), Mercury should exhibit swirls if the comet-impact models for lunar swirl formation were correct. Since Mercury apparently lacks swirls, the hypotheses for lunar swirls that invoke comet-related impacts are not favored. An additional objection to the comet-impact hypotheses is that the thin surface layer of regolith modified by the comet interaction would need an unrealistically high degree of magnetization in order to produce the magnetic fields observed (e.g., over the Reiner Gamma formation, Nicholas et al., 2007).

Hypotheses for lunar swirls that require direct interaction between the solar wind and a local crustal magnetic field are therefore preferred, and this recognition has implications regarding the phenomena responsible for "space weathering," the physical, chemical, and optical changes that result when regolith is exposed to the space environment on an airless body (e.g., Hapke, 2001). A soil that has accumulated more of these changes is said to be more "mature" than a soil with a lesser degree of exposure. The spectral changes that accompany space weathering include an overall reduction in reflectance (darkening), increase in visible-to-near-infrared spectral slope (reddening), and reduction in the contrast of absorption bands (e.g., Cassidy and Hapke, 1975; Fischer and Pieters, 1994; Pieters et al., 2000). These spectral changes are attributed to production of submicroscopic metallic iron blebs and coatings (also termed "nanophase iron", or npFe$^0$) on and within soil particles by reduction and vapor-phase deposition during solar-wind ion sputtering and/or micrometeoroid impact, as summarized by Hapke (2001). The relative importance of solar-wind sputtering versus micrometeoroid impact has been a matter of debate. If lunar crustal magnetic anomalies, which can generate mini-magnetospheres (Kurata et al., 2005; Halekas et al., 2008), are responsible for protecting soils from the process(es) that produce the optical effects associated with maturation, then by implication the solar wind is the key agent of space weathering on the Moon, because a magnetic anomaly would not screen out micrometeoroids (Richmond et al., 2003). Note that solar-wind ion bombardment is also thought to be the agent responsible for space weathering on asteroids (Hapke, 2001; Strazzulla et al., 2005; Vernazza et al., 2009).

If the magnetic-shielding or dust-levitation hypothesis for the origin of lunar swirls is correct, then the lack of swirls on Mercury

could imply that crustal magnetic anomalies of sufficient strength do not exist on the planet and/or that the solar wind is not the major agent of space weathering on Mercury. MESSENGER Magnetometer data from the first two flybys did not resolve local regions of magnetized crust on Mercury (Purucker et al., 2009), though data are limited to equatorial ground tracks. Mercury's global magnetic field should stand off the solar wind at most times (e.g., Anderson et al., 2008), with the degree of protection tending to vary with latitude (Hapke, 1977; Sarantos et al., 2007, 2009). Solar-wind ions are able to penetrate to the surface (e.g., Kallio and Janhunen, 2003), and during extreme tail-loading events such as those documented during MESSENGER's third flyby, all latitudes of the dayside surface are exposed to the solar wind (Slavin et al., 2010).

It may be that the rate of space weathering by micrometeoroid impact on Mercury exceeds that by solar wind bombardment. Cintala (1992) estimated that the micrometeoroid flux at Mercury is a factor of 5.5 greater than at the Moon. The average impact speed at Mercury is 1.6 times larger, resulting in ~14 times more impact melt and 20 times the production of vapor. Thus regolith maturation by the high flux of energetic micrometeoroids may outstrip the effects of solar-wind ion sputtering and implantation at Mercury.

If selective electrostatic dust transport is responsible for creating the lunar swirls, then less can be concluded regarding the agent of lunar space weathering. The rate of dust accumulation could be on shorter timescales than either solar wind or micrometeoroid weathering (Garrick-Bethell et al., 2010). Areas with accumulations of fine, bright dust within the magnetic anomaly may still be shielded from solar-wind ion implantation and sputtering, making it more difficult to separate the weathering effects of the solar wind from those of micrometeoroids. Future observations that can provide information on the grain size of swirl material will be important for testing the dust-levitation hypothesis.

## 6. Conclusions

1. Images returned by the MESSENGER spacecraft from the Mercury flybys have been examined in order to evaluate the possible presence of anomalous high-albedo markings similar to lunar swirls. Several features suggested to be swirls on the basis of Mariner 10 imaging (in the craters Handel and Lermontov) are revealed in higher-resolution MESSENGER images to lack the characteristic morphology of lunar swirls.
2. Basin-antipodal regions on the Moon are known to correlate with the presence of swirl-like albedo markings. The antipodes of several large impact basins on Mercury (Caloris, Rembrandt, Beethoven, and Tolstoj) appear to lack such unusual albedo markings.
3. The "hilly and lineated" terrain found at the antipode of Caloris, the largest young impact basin on Mercury, is absent at the Rembrandt, Beethoven, and Tolstoj antipodes. These basins may be too small to produce resolvable surface disturbances at their antipodes.
4. While albedo anomalies similar to lunar swirls have not been found on Mercury, the planet does possess its own class of unusual high-reflectance features. The bright crater-floor deposits (BCFDs) on Mercury are spectrally unique, implying the presence of material with an unusual composition or physical state. This characteristic is unlike the lunar swirls, which are predominantly visible because of maturity contrasts with their surroundings, with no evidence of unusual composition. Therefore the BCFDs are not analogs to the lunar swirls.
5. Cometary collisions should affect the surface of Mercury. The lack of swirls on Mercury is therefore evidence against hypotheses for the origin of lunar swirls that invoke comet-related impacts.
6. The apparent absence of lunar-type swirls on Mercury offers support to the hypotheses for the origin of lunar swirls that require interaction between the solar wind and a local crustal magnetic anomaly. If the solar-wind shielding model of swirl formation is correct, this would suggest that the primary agent responsible for the optical effects of space weathering on the Moon is the solar wind rather than micrometeoroid impact.

## Acknowledgments

Gratitude is extended to Jeffrey F. Bell (then of the University of Hawaii), who shared his unpublished notes on potential swirls in Mariner 10 images with the first author in the mid-1990s. Those notes inspired this work. The first author also appreciates discussions with Pete Schultz (Brown University) and C.G. Hughes (University of Pittsburgh). Jeffery Gillis-Davis (University of Hawaii) and Lon Hood (University of Arizona) provided very helpful informal reviews. We thank Bruce Hapke (University of Pittsburgh) and the anonymous reviewer for careful evaluations that led us to make improvements to this paper. Jay Dickson (Brown University) produced the image in Fig. 2b. This work made use of the Integrated Software for Imagers and Spectrometers (ISIS) and data obtained from the Map-a-Planet website (http://www.mapaplanet.org/), both maintained by the US Geological Survey's Astrogeology Team at Flagstaff, Arizona. The authors gratefully acknowledge financial support from the NASA Planetary Geology and Geophysics Program, the MESSENGER Participating Scientist Program, and the MESSENGER project, which is supported by the NASA Discovery Program under contracts NAS5-97271 to the Johns Hopkins University Applied Physics Laboratory and NASW-00002 to the Carnegie Institution of Washington.

## References

Anderson, B.J., Acuña, M.H., Korth, H., Purucker, M.E., Johnson, C.L., Slavin, J.A., Solomon, S.C., McNutt Jr., R.L., 2008. The structure of Mercury's magnetic field from MESSENGER's first flyby. Science 321, 82–85.

Becker, K.S., and 10 colleagues, 2009. Near global mosaic of Mercury. Eos Trans. AGU (Fall Suppl.) 90 (52). Abstract P21A-1189.

Bell, J.F., Hawke, B.R., 1981. The Reiner Gamma formation: Composition and origin as derived from remote sensing observations. Proc. Lunar Sci. Conf. 12, 679–694.

Bell, J.F., Hawke, B.R., 1987. Recent comet impacts on the Moon: The evidence from remote sensing studies. Publ. Astron. Soc. Pacific 99, 862–867.

Blewett, D.T., Hawke, B.R., Lucey, P.G., 2005. Lunar optical maturity investigations: A possible recent impact crater and a magnetic anomaly. J. Geophys. Res. 110, E04015. doi:10.1029/2004JE002380.

Blewett, D.T., Hawke, B.R., Lucey, P.G., Robinson, M.S., 2007. A Mariner 10 color study of mercurian craters. J. Geophys. Res. 112, E02005. doi:10.1029/2006JE002713.

Blewett, D.T., and 12 colleagues, 2008. Comparison of the color properties of selected features on Mercury from Mariner 10 and MESSENGER multispectral images. Eos Trans. AGU (Fall Suppl.) 89 (53). Abstract U21A-0023.

Blewett, D.T., Robinson, M.S., Denevi, B.W., Gillis-Davis, J.J., Head, J.W., Solomon, S.C., Holsclaw, G.M., McClintock, W.E., 2009. Multispectral images of Mercury from the first MESSENGER flyby: Analysis of global and regional color trends. Earth Planet. Sci. Lett. 285, 272–282.

Cassidy, W., Hapke, B., 1975. Effects of darkening processes on surfaces of airless bodies. Icarus 25, 371–383.

Chabot, N.L., Prockter, L.M., Murchie, S.L., Robinson, M.S., Laslo, N.R., Kang, H.K., Hawkins, S.E., Vaughan, R.M., Head, J.W., Solomon, S.C., 2008. Imaging during MESSENGER's second flyby of Mercury. Eos Trans. AGU (Fall Suppl.) 89 (53). Abstract U21A-0014.

Cintala, M.J., 1992. Impact-induced thermal effects in the lunar and mercurian regoliths. J. Geophys. Res. 97, 947–973.

Cintala, M.J., Grieve, R.A.F., 1998. Scaling impact melt and crater dimensions: Implications for the lunar cratering record. Meteor. Planet. Sci. 33, 889–912.

Coleman Jr., P.J., Schubert, G., Russell, G.T., Sharp, L.R., 1972. Satellite measurements of the Moon's magnetic field: A preliminary report. Moon 4, 419–429.

Denevi, B.W., Robinson, M.S., 2008. Mercury's albedo from Mariner 10: Evidence for the presence of ferrous iron. Icarus 197, 239–246.

Dzurisin, D., 1977. Mercurian bright patches: Evidence for physio-chemical alteration of surface material? Geophys. Res. Lett. 4, 383–386.

El-Baz, F., 1972. The Alhazen to Abul Wafa swirl belt: An extensive field of light-colored, sinuous markings. Apollo 16 Preliminary Science Report, SP-315, NASA, Washington, DC, pp. 29-93–29-97.

Fischer, E.M., Pieters, C.M., 1994. Remote determination of exposure degree and iron concentration of lunar soil using VIS–NIR spectroscopic methods. Icarus 111, 475–488.
Garrick-Bethell, I., Head, J.W., Pieters, C.M., 2009. Near-surface magnetic fields and dust transport at lunar swirls. Eos Trans. AGU (Fall Suppl.) 90 (52). Abstract GP34A-04.
Garrick-Bethell, I., Head, J.W., Pieters, C.M., 2010. Spectral properties of lunar swirls and their formation by dust transport. Lunar. Sci. 41. Abstract 2675.
Gold, T., Soter, S., 1976. Cometary impact and the magnetization of the Moon. Planet. Space Sci. 24, 45–54.
Halekas, J.S., Mitchell, D.L., Lin, R.P., Frey, S., Hood, L.L., Acuña, M.H., Binder, A.B., 2001. Mapping of crustal magnetic anomalies on the lunar near side by the Lunar Prospector electron reflectometer. J. Geophys. Res. 106, 27841–27852.
Halekas, J.S., Delory, G.T., Brain, D.A., Lin, R.P., Mitchell, D.L., 2008. Density cavity observed over a strong lunar crustal magnetic anomaly in the solar wind: A mini-magnetosphere? Planet. Space Sci. 56, 941–946.
Hapke, B., 1977. Interpretations of optical observations of Mercury and the Moon. Phys. Earth Planet. Inter. 15, 264–274.
Hapke, B., 2001. Space weathering from Mercury to the asteroid belt. J. Geophys. Res. 106, 10039–10073.
Hawkins III, S.E., and 24 colleagues, 2007. The Mercury Dual Imaging System on the MESSENGER spacecraft. Space Sci. Rev. 131, 247–338.
Head, J.W., and 10 colleagues, 2008. Volcanism on Mercury: Evidence from the first MESSENGER flyby. Science 321, 69–72.
Head, J.W., and 12 colleagues, 2009. Volcanism on Mercury: Evidence from the first MESSENGER flyby for extrusive and explosive activity and the volcanic origin of plains. Earth Planet. Sci. Lett. 285, 227–242.
Hood, L.L., Artemieva, N.A., 2008. Antipodal effects of lunar basin-forming impacts: Initial 3D simulations and comparisons with observations. Icarus 193, 485–502.
Hood, L., Schubert, G., 1980. Lunar magnetic anomalies and surface optical properties. Science 208, 49–51.
Hood, L., Williams, C., 1989. The lunar swirls: Distribution and possible origins. Proc. Lunar Sci. Conf. 19, 99–113.
Hood, L.L., Coleman, P.J., Wilhelms, D.E., 1979. Lunar nearside magnetic anomalies. Proc. Lunar Sci. Conf. 10, 2235–2257.
Hood, L.L., Russell, C.T., Coleman, P.J., 1981. Contour maps of lunar remanent magnetic fields. J. Geophys. Res. 86, 1055–1069.
Hood, L.L., Zakharian, A., Halekas, J., Mitchell, D.L., Lin, R.P., Acuña, M.H., Binder, A.B., 2001. Initial mapping and interpretation of lunar crustal magnetic anomalies using Lunar Prospector magnetometer data. J. Geophys. Res. 106, 27825–27839.
Hughes, H.G., App, F.N., McGetchin, T.R., 1977. Global seismic effects of basin-forming impacts. Phys. Earth Planet. Inter. 15, 251–263.
Kallio, E., Janhunen, P., 2003. Solar wind and magnetospheric ion impact on Mercury's surface. Geophys. Res. Lett. 30, 1877. doi:10.1029/2003GL017842.
Kaydash, V., Kreslavsky, M., Shkuratov, Y., Gerasimenko, S., Pinet, P., Josset, J.-L., Beauvivre, S., Foing, B., and the AMIE SMART-1 Team, 2009. Photometric anomalies of the lunar surface studied with SMART-1 AMIE data. Icarus 202, 393–413.
Kerber, L., Head, J.W., Solomon, S.C., Murchie, S.L., Blewett, D.T., Wilson, L., 2009. Explosive volcanic eruptions on Mercury: Eruption conditions, magma volatile content, and implications for interior volatile abundances. Earth Planet. Sci. Lett. 285, 263–271.
Kreslavsky, M.A., Shkuratov, Y.G., 2003. Photometric anomalies of the lunar surface: Results from Clementine data. J. Geophys. Res. 108, 5015. doi:10.1029/2002JE001937.
Kurata, M., Tsunakawa, H., Saito, Y., Shibuya, H., Matsushima, M., Shimizu, H., 2005. Mini-magnetosphere over the Reiner Gamma magnetic anomaly region on the Moon. Geophys. Res. Lett. 32, L24205. doi:10.1029/2005GL024097.
Le Feuvre, M., Wieczorek, M.A., 2008. Nonuniform cratering of the terrestrial planets. Icarus 197, 291–306.
Lin, R.P., Anderson, K.A., Hood, L., 1988. Lunar surface magnetic field concentrations antipodal to young large impact basins. Icarus 74, 529–541.
Marchi, S., Morbidelli, A., Cremonese, G., 2005. Flux of meteoroid impacts on Mercury. Astron. Astrophys. 431, 1123–1127.
McCauley, J.F., 1967. Geologic map of the Hevelius region of the Moon. Map I-491, Misc. Investigations Ser., US Geological Survey, Boulder, CO.
McClintock, W.E., Lankton, M.R., 2007. The Mercury Atmospheric and Surface Composition Spectrometer for the MESSENGER mission. Space Sci. Rev. 131, 481–521.
Melosh, H.J., 1989. Impact Cratering – A Geologic Process. Oxford University Press, New York. 245pp.
Moore, H.J., Hodges, C.A., Scott, D.H., 1974. Multiringed basins illustrated by Orientale and associated features. Proc. Lunar Sci. Conf. 5, 71–100.
Murchie, S.L., and 10 colleagues, 2008. Geology of the Caloris basin, Mercury: A view from MESSENGER. Science 321, 73–76.
Murray, B.C., Belton, M.J.S., Danielson, G.E., Davies, M.E., Gault, D.E., Hapke, B., O' Leary, B., Strom, R.G., Suomi, V., Trask, N., 1974. Preliminary description and interpretation from Mariner 10 pictures. Science 185, 169–179.
Nicholas, J.B., Purucker, M.E., Sabaka, T.J., 2007. Age spot or youthful marking: Origin of Reiner Gamma. Geophys. Res. Lett. 34, L02205. doi:10.1029/2006GL027794.
Pieters, C.M., Taylor, L.A., Noble, S.K., Keller, L.P., Hapke, B., Morris, R.V., Allen, C.C., McKay, D.S., Wentworth, S., 2000. Space weathering on airless bodies: Resolving a mystery with lunar samples. Meteor. Planet. Sci. 35, 1101–1107.
Pinet, P., Shevchenko, V., Chevrel, S., Daydou, Y., Rosemberg, C., 2000. Local and regional lunar regolith characteristics at Reiner Gamma formation: Optical and spectroscopic properties from Clementine and Earth-based data. J. Geophys. Res. 105, 9457–9475.
Prockter, L. M., and 12 colleagues, 2010. Evidence for young volcanism on Mercury from the third MESSENGER flyby. Science, in press.
Purucker, M.E., Sabaka, T.J., Solomon, S.C., Anderson, B.J., Korth, H., Zuber, M.T., Neumann, G.A., 2009. Mercury's internal magnetic field: Constraints on large- and small-scale fields of crustal origin. Earth Planet. Sci. Lett. 285, 340–346.
Rava, B., Hapke, B., 1987. An analysis of the Mariner 10 color ratio map of Mercury. Icarus 71, 397–429.
Richmond, N.C., Hood, L.L., Halekas, J.S., Mitchell, D.L., Lin, R.P., Acuña, M., Binder, A.B., 2003. Correlation of a strong lunar magnetic anomaly with a high-albedo region of the Descartes mountains. Geophys. Res. Lett. 30, 1395. doi:10.1029/2003GL016938.
Richmond, N.C., Hood, L.L., Mitchell, D.L., Lin, R.P., Acuña, M.H., Binder, A.B., 2005. Correlations between magnetic anomalies and surface geology antipodal to lunar impact basins. J. Geophys. Res. 110, E05011. doi:10.1029/2005JE002405.
Robinson, M.S., Lucey, P.G., 1997. Recalibrated Mariner 10 color mosaics: Implications for mercurian volcanism. Science 275, 197–200.
Robinson, M.S., and 12 colleagues, 2008. Reflectance and color variations on Mercury: Regolith processes and compositional heterogeneity. Science 321, 66–69.
Russell, C.T., Coleman Jr., P.J., Fleming, B.K., Hilburn, L., Ioannidis, G., Lichtenstein, B.R., Schubert, G., 1975. The fine scale lunar magnetic field. Proc. Lunar Sci. Conf. 6, 2955–2969.
Sarantos, M., Killen, R.M., Kim, D., 2007. Predicting the long-term solar wind ion-sputtering source at Mercury. Planet. Space Sci. 55, 1584–1585.
Sarantos, M., Slavin, J.A., Benna, M., Boardsen, S.A., Killen, R.M., Schriver, D., Trávníček, P., 2009. Sodium-ion pickup observed above the magnetopause during MESSENGER's first Mercury flyby: Constraints on neutral exospheric models. Geophys. Res. Lett. 36, L04106. doi:10.1029/2008GL036207.
Schultz, P.H., 1976. Moon Morphology. University of Texas Press, Austin. 626pp.
Schultz, P.H., 1977. Endogenic modification of impact craters on Mercury. Phys. Earth Planet. Inter. 15, 202–219.
Schultz, P.H., Gault, D.E., 1975. Seismic effects from major basin formation on the Moon and Mercury. Moon 12, 159–177.
Schultz, P.H., Srnka, L.J., 1980. Cometary collisions with the Moon and Mercury. Nature 284, 22–26 (See also "Reply" in Nature 287, 86–87).
Shkuratov, Y., Kaydash, V., Gerasimenko, S., Opanasenko, N., Velikodsky, Yu., Korokhin, V., Videen, G., Pieters, C., 2010. Probable swirls detected as photometric anomalies in Oceanus Procellarum. Icarus, in press. doi:10.1016/j.icarus.2010.01.028.
Slavin, J.A., and 18 colleagues, 2010. MESSENGER observations of extreme loading and unloading of Mercury's magnetic tail. Science, in press.
Solomon, S.C., and 10 colleagues, 2008. Return to Mercury: A global perspective on MESSENGER's first Mercury flyby. Science 321, 59–62.
Spudis, P.D., 1993. The Geology of Multi-Ring Impact Basins: The Moon and other Planets. Cambridge University Press, Cambridge, UK. 263pp.
Spudis, P.D., Guest, J.E., 1988. Stratigraphy and geologic history of Mercury. In: Vilas, F., Chapman, C.R., Matthews, M.S. (Eds.), Mercury. University of Arizona Press, Tucson, Arizona, pp. 118–164.
Starukhina, L., Shkuratov, Y., 2004. Swirls on the Moon and Mercury: Meteoroid swarm encounters as a formation mechanism. Icarus 167, 136–147.
Strazzulla, G., Dotto, E., Binzel, R., Brunetto, R., Barucci, M.A., Blancoe, A., Orofino, V., 2005. Spectral alteration of the meteorite Epinal (H5) induced by heavy ion irradiation: A simulation of space weathering effects on near-Earth asteroids. Icarus 174, 31–35.
Stuart-Alexander, D.E., 1978. Geologic map of the central far side of the Moon. Map I-1047, Misc. Investigations Ser., US Geological Survey, Denver, CO.
Vernazza, P., Binzel, R.P., Rossi, A., Fulchignoni, M., Birlan, M., 2009. Solar wind as the origin of rapid reddening of asteroid surfaces. Nature 458, 993–995.
Watters, T.R., Head, J.W., Solomon, S.C., Robinson, M.S., Chapman, C.R., Denevi, B.W., Fassett, C.I., Murchie, S.L., Strom, R.G., 2009. Evolution of the Rembrandt impact basin on Mercury. Science 324, 618–621.
Whitaker, E.A., 1969. Sublimates. In: Analysis of Apollo 8 Photography and Visual Observations, SP-201. NASA, Washington, DC, pp. 34–35.
Wieczorek, M.A., Zuber, M.T., 2001. A Serenitatis origin for the Imbrium grooves and South Pole-Aitken thorium anomaly. J. Geophys. Res. 106, 27,853–27,864.
Wilhelms, D.E., 1987. The Geologic History of the Moon. Prof. Paper 1348. US Geological Survey, Denver, CO, 302pp.